ACS APPLIED MATERIALS & INTERFACES

Research Article

www.acsami.org

Nanoporous Anodic Alumina Rugate Filters for Sensing of Ionic Mercury: Toward Environmental Point-of-Analysis Systems

Tushar Kumeria,[†] Mohammad Mahbubur Rahman,[†,‡] Abel Santos,*[,†] Josep Ferré-Borrull,[‡] Lluís F. Marsal,[‡] and Dusan Losic[†]

[†]School of Chemical Engineering, The University of Adelaide, Adelaide, SA 5005, Australia

[‡]Departament d'Enginyeria Electrònica, Elèctrica i Automàtica, Universitat Rovira i Virgili, Avda Països Catalans 26, 43007 Tarragona, Spain

Supporting Information

ABSTRACT: Herein, we present an ultrasensitive, cost-competitive, and portable optical sensing system for detecting ionic mercury in environmental water. This analytical system combines structurally engineered and chemically modified nanoporous anodic alumina rugate filters (NAA-RFs) with reflection spectroscopy (RfS). The sensing performance of the proposed system is assessed through several tests, establishing its sensing performance (i.e., linear working range from 1 to 100 μM of Hg^{2+}, low limit of detection 1 μM of Hg^{2+} ions (i.e., 200 ppb), and sensitivity of 0.072 nm μM^{-1}), chemical selectivity (i.e., exposure to different metal ions Co^{2+}, Mg^{2+}, Ni^{2+}, Cu^{2+}, Pb^{2+}, Fe^{3+}, Ca^{2+}, Cr^{6+}, and Ag^{+}) and metal ions binding mechanism (i.e., fitting to Langmuir and Freundlich isotherm models). Furthermore, the detection of Hg^{2+} ions in tap and environmental water (River Torrens) is successfully carried out, demonstrating the suitability of this system for developing environmental point-of-analysis systems.

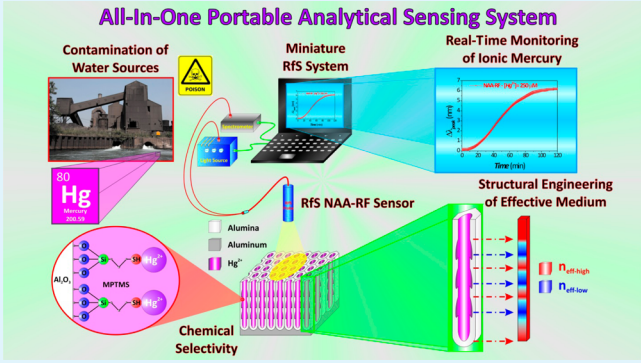

KEYWORDS: *nanoporous anodic alumina, reflection spectroscopy, optical rugate filters, mercury ions, selective surface chemistry, environmental water*

1. INTRODUCTION

Mercury emissions and releases produced by anthropogenic and natural sources have been accumulated in the natural environment by tropospheric cycling since the industrialization period in the 19th century.[1] Mercury can damage the immune and nervous systems, produce genetic mutations in developing embryos and affect motion coordination, touch, taste, and sight in adults.[2] Recently, worldwide concerns about mercury have been expressed by UNEP through a legally binding convention directed at controlling, monitoring and reducing mercury pollution at global scale.[3] In that regard, the development of ultrasensitive, handy, and cost-competitive sensors for monitoring levels of mercuric pollutants in water sources can enable effective actions to reduce levels of ionic mercury at opportune time, assessing risks for human populations and the environment.[1] Inorganic mercury(II) ions (Hg^{2+}) are the largest mercuric pollutants in environmental water and sources must be monitored throughout. Traditionally, atomic absorption spectroscopy (AAS) and gas chromatography (GC) have been used for this purpose since they can detect traces of ionic mercury (i.e., up to 10^{-7} wt % = 100 ppb; ppb = parts per billion).[4,5] More recently, surface enhanced Raman spectroscopy and plasmon enhanced vibrational spectroscopy have demonstrated outstanding sensing performances when detecting Hg^{2+} concentrations below 1 ppt (i.e., 10^{-12} wt % = 1 ppt; ppt = parts per trillion).[6−8] However, these techniques are expensive and require samples to be chemically treated before the analysis is performed, making it cost-intensive, laborious, and complicated. These limitations can be overcome by miniature spectrometers, which provide not only portability but also outstanding performances in terms of sensitivity, accuracy, and versatility. Amid the different optical techniques, reflection spectroscopy (RfS) has demonstrated competent capabilities in terms of limit of detection, accuracy and versatility for different sensing applications.[9−12] Moreover, RfS can be implemented in miniature spectrometers, reducing both costs and time consumed by current analytical techniques and enabling the development of portable point-of-analysis systems for detecting low levels of mercury in the site of interest (e.g., water sources).[13,14] RfS is an optical technique based on the constructive reflection of white light with a thin film, which can be combined with nanoporous structures such as porous silicon (PSi) and nanoporous anodic alumina (NAA). PSi and NAA are nanoporous materials that can confine, guide,

Received: May 12, 2014
Accepted: July 8, 2014
Published: July 8, 2014

   dx.doi.org/10.1021/am502882d | ACS Appl. Mater. Interfaces 2014, 6, 12971−12978

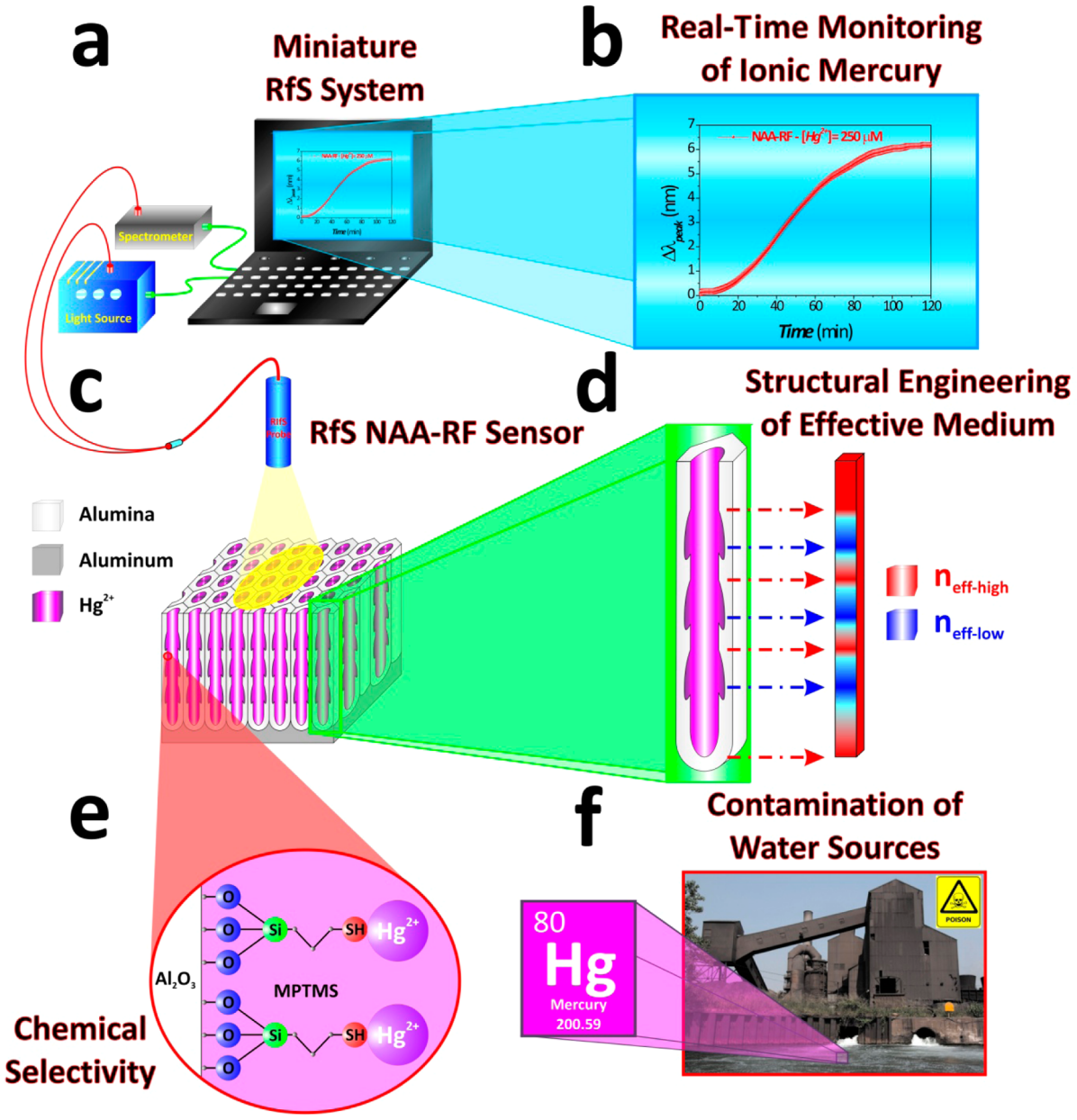

Figure 1. Scheme of proposed optical system for sensing Hg^{2+} in environmental water by combining RfS with structurally engineered and chemically modified NAA-RFs. (a) Miniature RfS system composed of notebook, light source, spectrometer, and optical probe. (b) Real-time monitoring of ionic mercury by RfS+NAA-RF system. (c) Optical sensing platform based on chemically modified NAA-RFs. (d) Structural engineering of effective medium in NAA-RFs. (e) Surface chemical selectivity by functionalization with MPTMS. (f) Real-time and label-free analysis of environmental water sources.

reflect and transmit light. Furthermore, their nanopores can be used as containers to accommodate molecules as well as chemical and physical filters for analytes. These properties can be achieved by engineering their nanoporous structure and changing their surface chemistry via functionalization, respectively.[15−24] Pore geometry in PSi and NAA can be structurally engineered by the etching/anodization parameters. Therefore, the effective medium of these nanoporous materials can be designed to produce a broad range of optically active structures (e.g., distributed Bragg reflectors, omnidirectional mirrors, rugate filters, waveguides, microcavities, etc.). For instance, rugate filters are optical nanostructures with effective refractive index modified in a sinusoidal or pseudosinusoidal manner in depth. These nanostructures present well-defined stop bands, where light is efficiently reflected in some narrow regions of the UV−visible−NIR spectrum. These stop bands can be established by tuning the pore geometry, yielding equidistant and well-defined isolated peaks in the reflection spectrum without sidebands. These peaks can be readily used to develop highly sensitive and selective optical sensors given that changes in the effective medium are translated into shifts in the position of the characteristic reflection peak of the optical rugate filter (i.e., sensing principle). Thus far, many studies have demonstrated that PSi is an excellent material to develop rugate filters.[18−27] Nonetheless, it is worth stressing that rugate filters based on NAA could offer many advantages; tunable pore geometry, cost-efficient, and scalable fabrication process and chemical and mechanical stability. NAA has been intensively

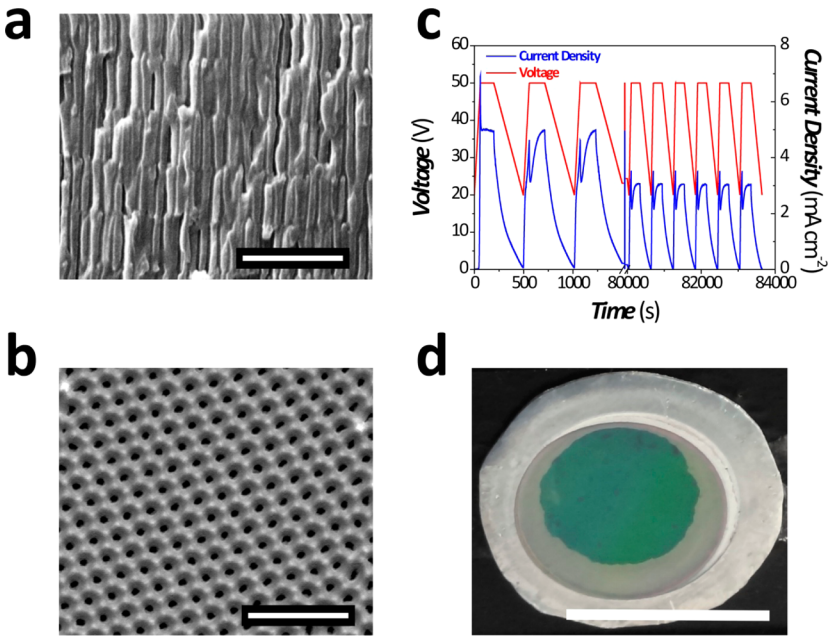

Figure 2. Fabrication and structural characteristics of NAA-RFs. (a) Cross-section SEM image of NAA-RFs fabricated in this study (scale bar = 1 μm). (b) Top-view SEM image of NAA-RFs (scale bar =500 nm). (c) Pseudosinusoidal anodization profile of NAA-RFs produced in this study. (d) Digital photography of NAA-RFs used in this study (scale bar = 1 cm).

used during the last years for a broad range of applications such as solar energy,[28,29] template synthesis,[30−34] and biosensing.[35−37]

In this scenario, we present for the first time an innovative portable and cost-competitive sensing system that combines chemically modified nanoporous anodic alumina rugate filters (NAA-Rfs) with RfS for sensing Hg^{2+} ions in environmental water. Figure 1 illustrates the proposed point-of-analysis system, which combines NAA-RFs and RfS for detecting Hg^{2+}.

2. EXPERIMENTAL SECTION

2.1. Materials. Aluminum (Al) foils of thickness 0.32 mm and purity 99.9997% were supplied by Goodfellow Cambridge Ltd. (UK). Oxalic acid ($C_2H_2O_4$), phosphoric acid (H_3PO_4), hydrochloric acid (HCl), ethanol (C_2H_5OH), acetone ($(CH_3)_2CO$), perchloric acid ($HClO_4$), hydrogen peroxide (H_2O_2), chromium trioxide (CrO_3), 3-(mercaptopropyl)-trimethoxysilane (MPTMS), cobalt(II) chloride ($CoCl_2$), magnesium(II) chloride ($MgCl_2$), nickel(II) sulfate ($NiSO_4$), copper(II) chloride ($CuCl_2$), lead(II) nitrate ($Pb(NO_3)_2$), iron(III) chloride ($FeCl_3$), calcium(II) chloride ($CaCl_2$), silver(I) nitrate ($AgNO_3$), and mercury(II) chloride ($HgCl_2$) were obtained from Sigma-Aldrich (Australia) and used as received. All solutions used in this study were prepared with ultrapure water Option Q-Purelabs (Australia).

2.2. Fabrication of NAA-RFs. Anodization of high purity Al foils by a modified two-step anodization process yields nanoporous anodic alumina rugate filters.[38−41] First, Al chips 1.5 cm in diameter were sonicated in ethanol (EtOH) and distilled water for 15 min each and dried under nitrogen stream. Then. aluminum chips were electropolished in a mixture of EtOH and $HClO_4$ 4:1 (*v*/*v*) at 20 V and 5 °C for 3 min. Subsequently, the first anodization step was conducted in a 0.3 M solution of $H_2C_2O_4$ at 40 V and 8 °C for 20 h and the resulting NAA was selectively removed by chemically etching in a mixture of 0.2 M chromic acid (H_2CrO_4) and 0.4 M H_3PO_4 at 70 °C for 3 h. After that, the second anodization step was carried out using the same acid electrolyte at 8 °C. In this step, however, a pseudosinusoidal anodization profile was applied. This step was not controlled by time but by total charge. Note that the remaining aluminum substrate was removed from the bottom side of these Al chips by chemical etching in mixture of hydrochloric acid and cupric chloride (HCl/$CuCl_2$). Finally, the nanoporous structure was widened by wet chemical etching in H_3PO_4 5 wt % at 35 °C for 18 min.

2.3. Functionalization of NAA-RFs. NAA-RFs were modified with MPTMS to chemically functionalize the inner surface of nanopores with thiol functional groups. Silanization was carried out through a well-established protocol reported elsewhere.[42] Briefly, hydroxyl groups (−OH) were generated on the inner surface of NAA-RFs by treatment with H_2O_2 30 wt % for 10 min at 85 °C. Then, NAA-RFs were dried under nitrogen stream prior to functionalization via chemical vapor deposition of MPTMS at 135 °C for 3 h. Physisorbed MPTMS molecules were removed from the surface of MPTMS-functionalized NAA-RFs by washing with acetone and water. Silanization was verified by Fourier transform infrared spectroscopy (FTIR, Nicolet 6700, Thermo Fisher Scientific, Australia) in the spectral range from 1000 to 3500 cm^{-1} (Figure S1, Supporting Information).

2.4. Optical RfS System. RfS spectra of NAA-RFs were acquired in real-time using a RfS system combined with a flow cell. This system consists of a bifurcated optical probe that conducts white light from a tungsten source (LS-1LL, Ocean Optics, USA) and focus it on NAA-RFs. The reflected light is collected by the collection fiber, which is assembled in the same optical probe. Finally, the reflected light is collected in a miniature spectrophotometer (USB 4000, Ocean Optics, USA). UV−visible optical spectra were acquired in the 400−1000 nm wavelength range. Spectral data were saved at intervals of 30 s with an integration time of 100 ms and 50 average measurements (i.e., time between two consecutive scans = 5 s). After collection, RfS spectra were processed by measuring the shift in the position of the reflection peak ($\Delta\lambda_{peak}$) in Igor Pro library (Wavemetrics, USA). $\Delta\lambda_{peak}$ was used as the sensing parameter and its changes were monitored in real-time to follow the binding of Hg^{2+} ions to thiol functional groups of MPTMS functionalities inside the NAA-RFs used in this study.

2.5. Flow Cell and Injection of Analyte Solutions. Sensing experiments were carried out by packing MPTMS-modified NAA-RFs in a flow cell based on acrylic plastic, through which the different analyte solutions were flowed by a peristaltic pump (BT100-2J, LongerPump, U.S.A.) at a constant flow rate of 400 μL min^{-1}. Prior to injection of the different analyte solutions, a stable baseline with the corresponding solvent (i.e., ultrapure, tap or River Torrens' water) was obtained for 10 min. The binding between Hg^{2+} ions and thiol functional groups inside the pores of MPTMS-modified NAA-RFs

produced shifts in $\Delta\lambda_{peak}$, which lasted until the available thiol groups on the inner surface of NAA-RFs were saturated with Hg^{2+} ions.

2.6. Chemical Selectivity Tests. The chemical selectivity of the proposed sensing system toward Hg^{2+} ions was assessed by exposing a MPTMS-modified NAA-RF sensor to 2 mM aqueous solutions of nine different metal ions (i.e., Co^{2+}, Mg^{2+}, Ni^{2+}, Cu^{2+}, Pb^{2+}, Fe^{3+}, Ca^{2+}, Cr^{6+}, and Ag^{+}), which was followed by a solution of Hg^{2+} ions with a fifty-fold lower concentration (i.e., 40 μM).

2.7. Applicability of RfS Combined with NAA-RFs for Real-Life Applications. To demonstrate the capability of the proposed sensing system for real-life environmental applications, MPTMS-modified NAA-RFs were analyzed when detecting Hg^{2+} ions (i.e., 5 and 40 μM) in tap and River Torrens' water. Whereas tap water was directly collected from the laboratory sink (SA Water, South Australia, Adelaide), environmental water was first collected from the River Torrens (Adelaide, South Australia, Australia) and thus filtered with a paper filter to remove any particulate. Water from these sources was used as a solvent for preparing 5 and 40 μM Hg^{2+} solutions used in these tests.

2.8. Structural Characterization of NAA-RFs. NAA-RFs were structurally characterized by analyzing SEM images, which were acquired by field emission gun scanning electron microscopy (FEG-SEM FEI Quanta 450).

Note that all the aforementioned experiments were repeated three times using freshly produced NAA-RFs.

3. RESULTS AND DISCUSSION

3.1. Fabrication of Optical NAA Rugate Filters. NAA-RFs were produced by anodization of Al foils following a modified two-step process. The second anodization step of this process consisted in a pseudosinusoidal voltage profile controlled by total charge (Q).[43,44] This process started at 20 V and, subsequently, the voltage was increased from 20 to 50 V at a rate of 0.5 V s^{-1}. After this, the anodization voltage was kept constant at 50 V for a charge of 1 C. Next, the anodization voltage was reduced from 50 to 20 V by a linear decreasing ramp at a rate of −0.01 V s^{-1}. This cycle was repeated 150 times. The anodization process was finished at the end of the decreasing voltage ramp of the last cycle. Note that anodization of aluminum is controlled by the flow of ionic species (i.e., OH^{-}, O^{2-}, Al^{3+}, etc.) across the oxide barrier layer at the pore bottom tips.[45] This electrochemical process enables the generation of optical nanostructures by engineering the effective medium in depth. This makes it possible to produce nanoporous platforms suitable for developing optical sensing systems. Figures 2a and b show top and cross-section views scanning electron microscopy (SEM) images of the resulting NAA-RFs. This reveals how the pore structure is engineered in depth by the anodization profile. Figure 2c presents the pseudosinusoidal anodization profile used in this study to produce NAA-RFs with optimal RfS signal. It is worthwhile mentioning that these NAA-RFs presented green color as a result of the reflected light. Figure 2d shows a digital photography of a NAA-RF demonstrating this optical phenomenon.

3.2. Optical Sensing Performance of NAA-RFs for Detection of Ionic Mercury. *3.2.1. Sensing Principle.* As mentioned before, in NAA-RFs, an increment of the effective medium yields a red shift in the reflection peak position (i.e., shift toward longer wavelengths = sensing principle). The sensing performance of these nanostructures was assessed by measuring shifts in the reflection peak position as a result of mercury ions binding. This process was monitored in real-time by RfS. Supporting Information Figure S2 shows an example of reflection spectrum of a NAA-RF in RfS obtained by shining white light on its surface and the red shift in $\Delta\lambda_{peak}$ before and after filling its nanopores with ethanol.

3.2.2. Real-Time Monitoring of Hg^{2+}. A set of NAA-RFs was chemically modified with MPTMS, which is an organosilane with thiol functional terminal (−SH), to endow NAA-RFs with chemical selectivity toward Hg^{2+} ions.[42] It is well-known that thiol groups have strong affinity for mercury ions. In particular, thiols are known as mercaptans becaue of their ability for mercury capture, forming a strong coordination complex with Hg^{2+}. Figure 3a presents an example of real-time monitoring of

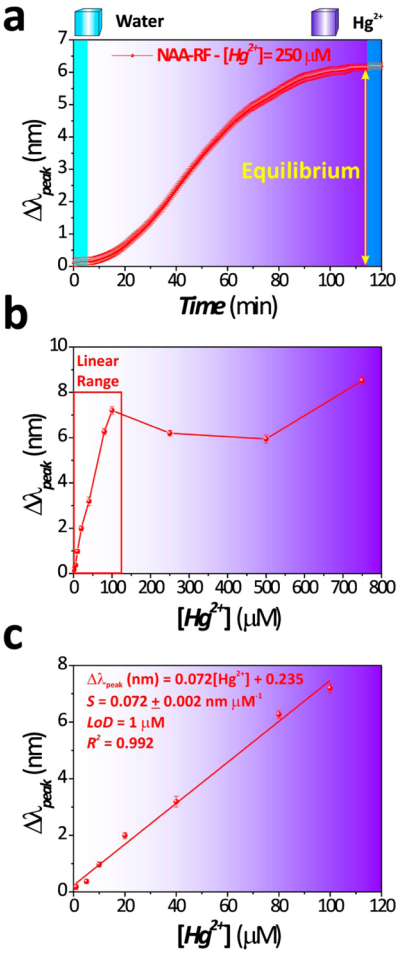

Figure 3. Sensing performance of the proposed sensing system for real-time detection of ionic mercury in ultrapure water. (a) Example of real-time monitoring of $\Delta\lambda_{peak}$ for [Hg^{2+}] = 250 μM. (b) $\Delta\lambda_{peak}$ as a function of analyte concentration from 1 to 750 μM. (c) Linear range of the proposed NAA-RF sensor, calibration curve and sensing parameters (i.e., from 1 to 100 μM). S = Sensitivity expressed in units of $\Delta\lambda_{peak}$ per concentration of analyte in mM. LoD = Low analyte concentration out of the standard deviation of the fitting line. R^2 = Linearity.

$\Delta\lambda_{peak}$ by RfS for detection of 250 μM Hg^{2+} in ultrapure water. It is worth noting that a stable $\Delta\lambda_{peak}$ baseline was first obtained with ultrapure water for 10 min, which was followed by injection of the analyte solution into the flow cell. After this, a sharp shift of approximately 6 nm in λ_{peak} was observed when the MPTMS-modified NAA-RF was exposed to the analyte solution. This confirmed the binding of Hg^{2+} ions to thiol terminals of MPTMS molecules present on NAA-RF pores. Stress that, after $\Delta\lambda_{peak}$ achieved a stable value, ultrapure water

Table 1. Characteristic Constants and Correlation Coefficients for Langmuir and Freundlich Binding Isotherm Models Obtained for the Immobilization and Detection of Mercury Ions in the Proposed Optical Sensing System

Langmuir model			Freundlich model		
$\Delta\lambda^{m}_{peak}$ (nm)	K_L (μM^{-1})	R^2	K_f (mg g^{-1})	n^{-1}	R^2
8.3 ± 0.7	0.015 ± 0.007	0.942	0.23 ± 0.02	0.61 ± 0.08	0.875

was flowed again through the flow cell in order to remove nonspecifically bound Hg^{2+} ions. Then, $\Delta\lambda_{peak}$ remained stable at that value throughout. In this way, we ensured that the total shift in $\Delta\lambda_{peak}$ was a result of an increase in the effective medium of the MPTMS-modified NAA-RF, which is associated with a stable binding of Hg^{2+} ions over the inner surface of NAA-RFs. Following this procedure and using $\Delta\lambda_{peak}$ as the sensing parameter, we assessed the performance of the proposed system for detecting ionic mercury in ultrapure water as a function of the analyte concentration (i.e., $[Hg^{2+}]$). To this end, $[Hg^{2+}]$ was modified from 1 to 750 μM and $\Delta\lambda_{peak}$ was monitored in real-time for each of these samples. From this, we obtained a calibration curve that correlates $\Delta\lambda_{peak}$ with $[Hg^{2+}]$. Ten different concentrations of Hg^{2+} ions within 3 orders of magnitude (i.e., from 1 to 750 μM) were evaluated to establish the linear and saturation range of the proposed sensing device. Figure 3b shows that $\Delta\lambda_{peak}$ saturates at concentrations above 100 μM. This suggests that the binding sites (i.e., thiol terminal groups) for Hg^{2+} ions on the MPTMS-modified NAA-RFs get saturated of mercury ions above that concentration. A linear relationship between $\Delta\lambda_{peak}$ and $[Hg^{2+}]$, however, was observed from 1 to 100 μM (i.e., from 200 ppb to 20 ppm; ppm = parts per million). A linear fitting of $\Delta\lambda_{peak}$ with the analyte concentration within this concentration range is presented in Figure 3c along with the resulting fitting equation and the sensing parameters. This calibration curve can be used to quantify concentrations of Hg^{2+} ions in aqueous solutions by measuring $\Delta\lambda_{peak}$ in the proposed sensing system, which presents a sensitivity (S) of 0.072 nm μM^{-1}, a low limit of detection (LoD) of 1 μM and a linearity (R^2) of 0.992 within a broad analyte concentration range (i.e., from 1 to 100 μM).

3.2.3. Isotherm Models for Binding of Hg^{2+} Ions over MPTMS-Modified NAA-RFs. The obtained results were fitted to Langmuir and Freundlich isotherm models to figure out the kinetics binding mechanism between Hg^{2+} ions and thiol groups on the inner surface of chemically functionalized NAA-RFs.[46] A complete mathematical derivation for these isotherm models is provided in the Supporting Information.

Langmuir isotherm model for the studied process is given by eq 1.

$$\frac{[Hg^{2+}]}{\Delta\lambda^{e}_{peak}} = \frac{1}{K_L\Delta\lambda^{m}_{peak}} + \frac{[Hg^{2+}]}{\Delta\lambda^{m}_{peak}} \quad (1)$$

where $\Delta\lambda^{e}_{peak}$ is the shift in the reflection peak position at equilibrium (see Figure 3a) and K_L and $\Delta\lambda^{m}_{peak}$ are characteristic constants.

Therefore, $1/(K_L\Delta\lambda^{m}_{peak})$ and $1/(\Delta\lambda^{m}_{peak})$ can be obtained by a linear fitting between $\Delta\lambda^{e}_{peak}$ and $[Hg^{2+}]$.

As for the Freundlich isotherm model adapted to the binding of mercury ions, this is given by eq 2.

$$\log(\Delta\lambda^{e}_{peak}) = \log(K_f) + \frac{1}{n}\log([Hg^{2+}]) \quad (2)$$

where K_f and n are characteristic constants.

Hence, values of $\log(K_f)$and $1/n$ can be estimated by the intercept and slope of a linear fitting between $\log(\Delta\lambda^{e}_{peak})$ and $\log([Hg^{2+}])$, respectively.

Note that, while Langmuir isotherm model describes flat surfaces considering constant the number of binding sites throughout the reaction (i.e., functional groups on the inner surface of NAA-RF), Freundlich isotherm model characterizes rough surfaces, assuming that the number of binding sites increases with the concentration of analyte molecules (i.e., $[Hg^{2+}]$). To throw light on this question, experimental data were fitted to both isotherm models and their characteristic constants calculated. The obtained results and the correlation factors are summarized in Table 1. The fitting parameters reveal that the binding mechanism between mercury ions and thiol groups on the surface of NAA-RFs can be described by a Langmuir isotherm model. Supporting Information Figure S3 shows a graphic of the obtained Langmuir and Freundlich isotherm models. It was observed that the experimental data fitted better to a Langmuir isotherm model. These results indicate that the binding of Hg^{2+} ions in the sensing platform follows a monolayer sorption mechanism.

Finally, an additional control test was carried out to demonstrate that changes in $\Delta\lambda_{peak}$ were exclusively associated with selective binding of Hg^{2+} ions to thiol groups. To this end, an as-produced NAA-RF (i.e., NAA-RF without MPTMS functionalization) was exposed to a 40 μM aqueous solution of Hg^{2+} ions (Figure S4, Supporting Information). These results demonstrate that changes in $\Delta\lambda_{peak}$ for NAA-RFs without MPTMS functionalization are negligible as compared to NAA-RFs functionalized with MPTMS.

3.2.4. Chemical Selectivity of NAA-RFs toward Hg^{2+}. The chemical selectivity of the presented optical sensing system was analyzed by a series of selectivity tests, in which a MPTMS-modified NAA-RF was exposed to a succession of 2 mM aqueous solutions of Co^{2+}, Mg^{2+}, Ni^{2+}, Cu^{2+}, Pb^{2+}, Fe^{3+}, Ca^{2+}, Cr^{6+}, and Ag^{+} ions, which are common ions present in environmental water. This was followed by final injection of an aqueous solution of 40 μM Hg^{2+} ions. These interfering metal ions were selected as common ions in environmental water, which present low (i.e., Fe^{3+} and Mg^{2+}) and high (i.e., Ag^{+}) affinity toward thiol functional groups. Figure 4a shows a bar graph of $\Delta\lambda_{peak}$ for the aforementioned test. This demonstrates that the highest nonspecific change in $\Delta\lambda_{peak}$ was observed for Ag^{+} and Cu^{2+} analytes (i.e., 1.52 ± 0.04 and 0.66 ± 0.01 nm, respectively). However, when the same sample was exposed to a 40 μM aqueous solution of Hg^{2+} (i.e., concentration 50 times lower), a sharp change in $\Delta\lambda_{peak}$ of 3.20 ± 0.20 nm was observed. This result proves that the proposed optical sensing system is highly selective toward ionic mercury in complex mixtures of metal ions.

3.2.5. Detection of Hg^{2+} in Tap and Environmental Water. To assess the suitability of the proposed optical sensing system for detecting ionic mercury in real-life environmental applications, two model solutions of Hg^{2+} (i.e., 5 and 40 μM) were prepared in tap water (i.e., SA Water, Adelaide) and environmental water collected from a local river (i.e., River

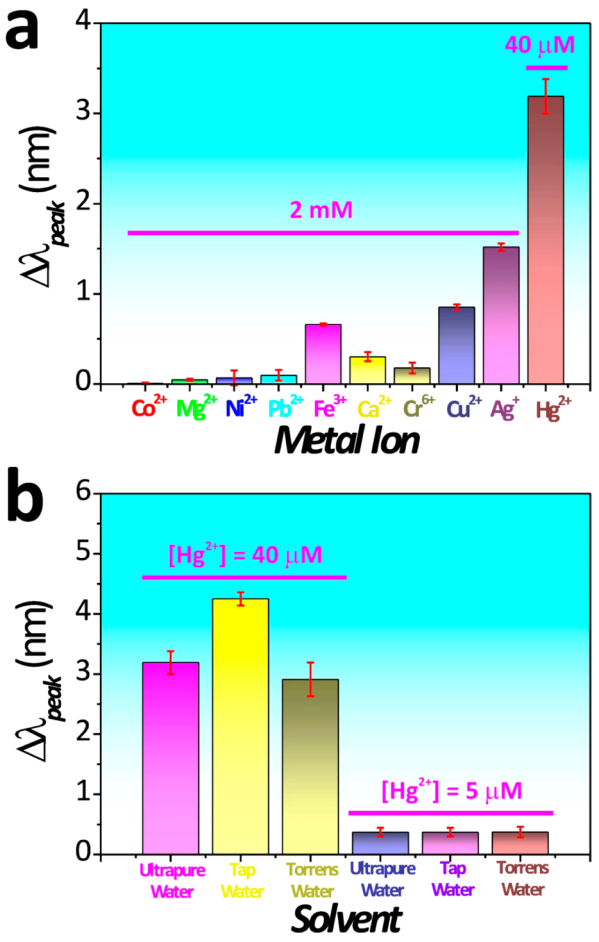

Figure 4. Chemical selectivity and real-life application of the proposed optical sensing system. (a) Bar graph chart showing $\Delta\lambda_{peak}$ after exposure to aqueous solutions of different metal ions. (b) Bar graph chart showing $\Delta\lambda_{peak}$ on exposing a MPTMS-modified NAA-RFs to 5 and 40 μM Hg^{2+} solutions prepared in ultrapure, tap and River Torrens' water, respectively.

Torrens, Adelaide). It is worth mentioning that in these experiments 5 and 40 μM aqueous solutions of Hg^{2+} prepared in ultrapure water were used as control samples. Moreover, a stable baseline was first obtained with the corresponding solvent (i.e., ultrapure, tap or River Torrens' water) for 10 min. After this, the analyte solutions of Hg^{2+} prepared in these solvents were injected into the flow cell. These solvents were also flowed at the end of these processes in order for obtaining the total change in $\Delta\lambda_{peak}$ associated with specific binding of mercury ions to thiol groups. The obtained results revealed that $\Delta\lambda_{peak}$ for 40 μM solutions of Hg^{2+} ions prepared in tap and River Torrens' water were 4.25 ± 0.11 and 2.91 ± 0.28 nm, respectively. This response is slightly higher and lower, respectively, as compared to 3.19 ± 0.19 nm for the same concentration of Hg^{2+} in ultrapure water (i.e., control sample) (Figure 4b). This slight difference in response could be associated with interactions from organic impurities and ionic compounds present in these complex solvents, which interfere slightly the binding affinity between Hg^{2+} ions and thiol functional groups. This difference in $\Delta\lambda_{peak}$, however, became smaller when the concentration of analyte was reduced to 5 μM. In that case, $\Delta\lambda_{peak}$ was the same for all these samples, 0.37 ± 0.07 nm. Examples of real-time RfS response curves for 40 μM Hg^{2+} ions in ultrapure and River Torrens' water are shown in Supporting Information Figure S5. This result verifies that the proposed optical system combined with MPTMS-modified NAA-RFs is able to carry out real-time and label-free detection of ionic mercury in environmental samples without further chemical treatments.

4. CONCLUSIONS

In summary, this study has demonstrated the capability of reflection spectroscopy combined with structurally engineered and chemically modified nanoporous anodic alumina rugate filters for real-time and label-free detection of ionic mercury in complex mixtures of metallic ions and environmental samples (i.e., tap and River Torrens' water). For the first time, NAA-RFs were structurally engineered and chemically modified to produce optical nanostructures with optimized effective medium for sensing applications. Chemical selectivity toward Hg^{2+} ions was achieved through thiol functional groups on MPTMS-modified NAA-RFs. The linear working range of the proposed system for detection of ionic mercury was from 1 to 100 μM, with a low limit of detection of 1 μM (i.e., 200 ppb) and a sensitivity of 0.072 nm μM^{-1}. Furthermore, the binding mechanism of Hg^{2+} ions to thiol functional groups inside the NAA-RF was found to follow a Langmuir isotherm model. Finally, the proposed RfS optical sensing system was capable of selectively detecting mercury ions in complex mixtures of metal ions and environmental samples (i.e., tap and River Torrens water). Although the obtained results are certainly promising and demonstrate the potential capabilities of the proposed system, these reveal that the performance of the proposed system is slightly above the highest mercury levels in drinking water established by the US environmental protection agency (EPA), which is 2 ppb. Nevertheless, it is worth stressing that there is a broad margin to improve the performance of the proposed system by enhancing the surface chemistry and structure of NAA rugate filters. For instance, different functional groups (e.g., oligonucleotides, oligopeptides, etc.) have shown better sensing performances than traditional thiol chemistry by providing more significant changes in the effective refractive index of the sensing platform when mercury ions are immobilized onto the nanoporous network.

The promising sensing performance of the proposed system along with its cost-competitive and scalable fabrication process of its sensing platforms (i.e., NAA-RFs) and portability make it an excellent alternative to current analytical techniques. This system could be at the base of future point-of-analysis systems for monitoring of the quality of environmental water in situ.

■ ASSOCIATED CONTENT

Supporting Information

Further information about FTIR spectra of MPTMS-modified NAA-RFs, the sensing principle of the proposed system, a complete mathematical derivation of Langmuir and Freundlich binding isotherms models, and a control test comparing as-produced and chemically modified NAA-RFs. This material is available free of charge via the Internet at http://pubs.acs.org.

■ AUTHOR INFORMATION

Corresponding Author

*Phone: +61 8 8313 1535. Fax: +61 8 8303 4373. E-mail: abel.santos@adelaide.edu.au. Web page: http://www.adelaide.edu.au/directory/abel.santos.

Author Contributions

T.K., M.M.R., and A.S. contributed equally to this work. The manuscript was written through contributions of all authors. All authors have given approval to the final version of the manuscript.

Notes

The authors declare no competing financial interest.

■ ACKNOWLEDGMENTS

This research was supported by the Australian Research Council (ARC) through the grants number FT110100711 and DE14010054, the Spanish Ministerio de Economía y Competitividad through the grant number TEC2012-34397 and the Generalitat de Catalunya through the grant number 2014 SGR 1344. Authors thank Mr. Jason Peak, Mr. Michael Jung, and Mr. Jeffrey Hiorns from the mechanical workshop of the School of Chemical Engineering (UoA) for their help and support with the fabrication of the experimental set-ups used in this study and the Adelaide Microscopy (AM) centre for FEG-SEM characterisation.

■ ABBREVIATIONS

NAA-RFs, nanoporous anodic alumina rugate filters
pSi, porous silicon
RfS, reflection spectroscopy
S, sensitivity
LoD, limit of detection

■ REFERENCES

(1) UNEP Chemicals Branch. In *UNEP Global Mercury Assessment 2013: Sources, Emissions, Releases and Environmental Transport*; UNEP: Geneva, Switzerland, 2013.

(2) Risher, J.; DeWoskin, R. In *Toxicological Profile for Mercury*; U.S. Department of Health and Human Services, Public Health Service, Agency for Toxic Substances and Disease Registry: Atlanta, GA, U.S.A., 1999.

(3) Kohler, P. M.; Morgera, E.; Ripley, K.; Schabus, N.; Tsioumani, E. Summary of The Fifth Session of The Intergovernmental Negotiating Committee to Prepare a Global Legally Binding Instrument on Mercury. *ENB* **2013**, *28*, 1−25.

(4) Hatch, W. R.; Ott, W. L. Determination of Sub-Microgram Quantities of Mercury by Atomic Absorption Spectrophotometry. *Anal. Chem.* **1968**, *40*, 2085−2087.

(5) Bloom, N.; Fitzgerald, W. F. Determination of Volatile Mercury Species at The Pictogram Level by Low-Temperature Gas Chromatography with Cold-Vapour Atomic Fluorescence Detection. *Anal. Chim. Acta* **1988**, *208*, 151−161.

(6) Zhang, L.; Chang, H.; Hirata, A.; Wu, H.; Xue, Q. K.; Chen, M. Nanoporous Gold Based Optical Sensor for Sub-ppt Detection of Mercury Ions. *ACS Nano* **2013**, *7*, 4595−4600.

(7) Ma, W.; Sun, M.; Xu, L.; Wang, L.; Kuang, H.; Xu, C. A SERS Active Gold Nanostar Dimer for Mercury Ion Detection. *Chem. Commun.* **2013**, *49*, 4989−4991.

(8) Hoang, C. V.; Oyama, M.; Saito, O.; Aono, M.; Nagao, T. Monitoring The Presence of Ionic Mercury in Environmental Water by Plasmon-Enhanced Infrared Spectroscopy. *Sci. Rep.* **2013**, *3*, 1175−1−3.

(9) Lin, V. S. Y.; Motesharei, K.; Dancil, K. P. S.; Sailor, M. J.; Ghadiri, M. R. A Porous Silicon-Based Optical Interferometric Biosensor. *Science* **1997**, *278*, 840−843.

(10) Santos, A.; Kumeria, T.; Losic, D. Optically Optimized Photoluminescent and Interferometric Biosensors Based on Nanoporous Anodic Alumina: A Comparison. *Anal. Chem.* **2013**, *85*, 7904−7911.

(11) Santos, A.; Balderrama, V. S.; Alba, M.; Formentín, P.; Ferré-Borrull, J.; Pallarès, J.; Marsal, L. F. Nanoporous Anodic Alumina Barcodes: Toward Smart Optical Biosensors. *Adv. Mater.* **2012**, *24*, 1050−1054.

(12) Kumeria, T.; Losic, D. Controlling Interferometric Properties of Nanoporous Anodic Aluminium Oxide. *Nanoscale Res. Lett.* **2012**, *7*, 88−1−10.

(13) Wang, G. L.; Zhu, X. Y.; Jiao, H. J.; Dong, Y. M.; Li, Z. J.; Li, Z. J. Ultrasensitive and Dual Functional Colorimetric Sensors for Mercury (II) Ions and Hydrogen Peroxide Based on Catalytic Reduction Property of Silver Nanoparticles. *Biosens. Bioelectron.* **2012**, *31*, 337−342.

(14) Wang, G. L.; Xu, X. F.; Cao, L. H.; He, C. H.; Li, Z. J.; Zhang, C. Mercury(II)-Stimulated Oxidase Mimetic Activity of Silver Nanoparticles as a Sensitive and Selective Mercury(II) Sensor. *RSC Adv.* **2014**, *4*, 5867−5872.

(15) Pacholski, C.; Sartor, M.; Sailor, M. J.; Cunin, F.; Miskelly, G. M. Biosensing Using Porous Silicon Double-Layer Interferometers: Reflective Interferometric Fourier Transform Spectroscopy. *J. Am. Chem. Soc.* **2005**, *127*, 11636−11645.

(16) Pacholski, C.; Yu, C.; Miskelly, G. M.; Godin, D.; Sailor, M. J. Reflective Interferometric Fourier Transform Spectroscopy: A Self-Compensating Label-Free Immunosensor Using Double-Layers of Porous SiO_2. *J. Am. Chem. Soc.* **2006**, *128*, 4250−4252.

(17) Orosco, M. M.; Pacholski, C.; Sailor, M. J. Real-Time Monitoring of Enzyme Activity in a Mesoporous Silicon Double Layer. *Nat. Nanotechnol.* **2009**, *4*, 255−258.

(18) Pavesi, L.; Dubos, P. Random Porous Silicon Multilayers: Application to Distributed Bragg Reflectors and Interferential Fabry-Pérot Filters. *Semicond. Sci. Technol.* **1997**, *12*, 570−575.

(19) Pellegrini, V.; Tredicucci, A.; Mazzoleni, C.; Pavesi, L. Enhanced Optical Properties in Porous Silicon Microcavities. *Phys. Rev. B: Condens. Matter Mater. Phys.* **1995**, *52*, R14 328−R14 328.

(20) Pavesi, L.; Guardini, R.; Mazzoleni, C. Porous Silicon Resonant Cavity Light Emitting Diodes. *Solid State Commun.* **1996**, *97*, 1051−1053.

(21) Cunin, F.; Schemedake, T. A.; Link, J. R.; Li, Y. Y.; Koh, J.; Bhatia, S. N.; Sailor, M. J. Biomolecular Screening with Encoded Porous-Silicon Photonic Crystals. *Nat. Mater.* **2002**, *1*, 39−41.

(22) Ilyas, S.; Böcking, T.; Kilian, K.; Reece, P. J.; Gooding, J. J.; Gaus, K.; Gal, M. Porous Silicon Based Narrow Line-Width Rugate Filters. *Opt. Mater.* **2007**, *29*, 619−622.

(23) Kilian, K. A.; Böcking, T.; Ilyas, S.; Gaus, K.; Jessup, W.; Gal, M.; Gooding, J. J. Forming Antifouling Organic Multilayers on Porous Silicon Rugate Filters towards In Vivo/Ex Vivo Biophotonic Devices. *Adv. Funct. Mater.* **2007**, *17*, 2884−2890.

(24) Li, Y. Y.; Cunin, F.; Link, J. R.; Gao, T.; Betts, R. E.; Reiver, S. H.; Chin, V.; Bhatia, S. N.; Sailor, M. J. Polymer Replicas of Photonic Porous Silicon for Sensing and Drug Delivery Applications. *Science* **2003**, *299*, 2045−2047.

(25) Shang, Y.; Wang, X.; Xu, E.; Tong, C.; Wu, J. Optical Ammonia Gas Sensor Based on a Porous Silicon Rugate Filter Coated with Polymer-Supported Dye. *Anal. Chim. Acta* **2011**, *685*, 58−64.

(26) Chapron, J.; Alekseev, S. A.; Lysenko, V.; Zaitsev, V. N.; Barbier, D. Analysis of Interaction between Chemical Agents and Porous Si Nanostructures Using Optical Sensing Properties of Infra-Red Rugate Filters. *Sens. Actuators, B* **2007**, *120*, 706−711.

(27) Pacholski, C.; Sailor, M. J. Sensing with Porous Silicon Double Layers: A General Approach for Background Suppression. *Phys. Status Solidi C* **2007**, *4*, 2088−2092.

(28) Mubeen, S.; Singh, N.; Lee, J.; Stucky, G. D.; Moskovits, M.; McFarland, E. W. Synthesis of Chemicals Using Solar Energy with Stable Photoelectrochemically Active Heterostructures. *Nano Lett.* **2013**, *13*, 2110−2115.

(29) Ghrib, M.; Ouertani, R.; Gaidi, M.; Khedher, N.; Salem, M. B.; Ezzaouia, H. Effect of Annealing on Photoluminescence and Optical Properties of Porous Anodic Alumina Films Formed in Sulfuric Acid for Solar Energy Applications. *Appl. Surf. Sci.* **2012**, *258*, 4995−5000.

(30) Sulka, G. D.; Brozózka, A.; Liu, L. Fabrication of Diameter-Modulated and Ultrathin Porous Nanowires in Anodic Aluminium Oxide Templates. *Electrochim. Acta* **2011**, *56*, 4972−4979.

(31) Claussen, J. C.; Wickner, M. M.; Fisher, T. S.; Porterfield, D. M. Transforming the Fabrication and Biofunctionalization of Gold Nanoelectrode Arrays into Versatile Electrochemical Glucose Biosensors. *ACS Appl. Mater. Interfaces* **2011**, *3*, 1765−1770.
(32) Sun, L.; Zhang, L.; Liang, C.; Yuan, Z.; Zhang, Y.; Xu, W.; Zhang, J.; Chen, Y. Chitosan Modified Fe^0 Nanowires in Porous Anodic Alumina and Their Application for The Removal of Hexavalent Chromium from Water. *J. Mater. Chem.* **2011**, *21*, 5877−5880.
(33) Franklin, A. D.; Janes, D. B.; Claussen, J. C.; Fisher, T. S.; Sands, T. D. Independently Addressable Fields of Porous Anodic Alumina Embedded in SiO_2 on Si. *Appl. Phys. Lett.* **2008**, *92*, No. 013122.
(34) Rana, K.; Kucukayan-Dogu, G.; Bengu, E. Growth of Vertically Aligned Carbon Nanotubes over Self-Ordered Nano-Porous Alumina Films and Their Surface Properties. *Appl. Surf. Sci.* **2012**, *258*, 7112−7117.
(35) Zhang, Z.; Wang, Q.; Li, G. Fabrication of Novel Nanoporous Array Anodic Alumina Solid-Phase Microextraction Fiber Coating and Its Potential Application for Headspace Sampling of Biological Volatile Organic Compounds. *Anal. Chim. Acta* **2012**, *727*, 13−19.
(36) Claussen, J. C.; Hengenius, J. B.; Wickner, M. M.; Fisher, T. S.; Umulis, D. M.; Porterfield, D. M. Effects of Carbon Nanotube-Tethered Nanosphere Density on Amperometric Biosensing: Simulation and Experiment. *J. Phys. Chem. C* **2011**, *115*, 20896−20904.
(37) Kumeria, T.; Rahman, M. M.; Santos, A.; Ferré-Borrull, J.; Marsal, L. F.; Losic, D. Structural and Optical Nanoengineering of Nanoporous Anodic Alumina Rugate Filters for Real-Time and Label-Free Biosensing Applications. *Anal. Chem.* **2014**, *86*, 1837−1844.
(38) Masuda, H.; Fukuda, K. Ordered Metal Nanohole Arrays Made by a Two-Step Replication of Honeycomb Structures of Anodic Alumina. *Science* **1995**, *268*, 1466−1468.
(39) Masuda, H.; Hasegwa, F. J. Self-Ordering of Cell Arrangement of Anodic Porous Alumina Formed in Sulfuric Acid Solution. *Electrochem. Soc.* **1997**, *144*, L127−L 130.
(40) Masuda, H.; Yada, K.; Osaka, A. Self-Ordering of Cell Configuration of Anodic Porous Alumina with Large-Size Pores in Phosphoric Acid Solution. *Jpn. J. Appl. Phys.* **1998**, *37*, L 1340−L1342.
(41) Nielsch, K.; Choi, J.; Schwirn, K.; Wehspohn, R. B.; Gösele, U. Self-Ordering Regimes of Porous Alumina: The 10% Porosity Rule. *Nano Lett.* **2002**, *2*, 677−680.
(42) Md Jani, A. M.; Kempson, I. M.; Losic, D.; Voelcker, N. H. Dressing in Layers: Layering Surface Functionalities in Nanoporous Aluminum Oxide Membranes. *Angew. Chem., Int. Ed.* **2010**, *49*, 7933−7937.
(43) Santos, A.; Formentín, P.; Pallarès, J.; Ferré-Borrull, J.; Marsal, L. F. Structural Engineering of Nanoporous Anodic Alumina Funnels with High Aspect Ratio. *J. Electroanal. Chem.* **2011**, *655*, 73−78.
(44) Rahman, M. M.; Garcia-Caurel, E.; Santos, A.; Marsal, L. F.; Pallarès, J.; Ferré-Borrull, J. Effect of The Anodization Voltage on The Pore-Widening Rate of Nanoporous Anodic Alumina. *Nanoscale Res. Lett.* **2012**, *7*, 474−1−7.
(45) Jessensky, O.; Müller, F.; Gösele, U. Self-Organized Formation of Hexagonal Pore Arrays in Anodic Alumina. *Appl. Phys. Lett.* **1998**, *72*, 1173−1175.
(46) Schwartz, M. P.; Alvarez, S. D.; Sailor, M. J. Porous SiO_2 Interferometric Biosensor for Quantitative Determination of Protein Interactions: Binding of Protein A to Immunoglobulins Derived from Different Species. *Anal. Chem.* **2007**, *79*, 327−334.